

Article

Biomechanics of helmet mask structures in mitigating explosion-induced traumatic brain injury: A numerical simulation study

Xuan Ma^{1,†}, Bin Yang^{1,*}, Yang Zheng^{2,†}, Feng Gao^{1,†}, Ronghua Zhou^{3,*}, Jiajia Zou¹, Xingyu Zhang¹¹ School of Transportation Engineering, Nanjing Institute of Technology, Nanjing 211167, China² School of Automotive and Traffic Engineering, Jiangsu University, Zhenjiang 212013, China³ Zhiwu Yunxiang (Nanjing) Information Technology Co., Ltd., Nanjing 210031, China* **Corresponding authors:** Bin Yang, yangb123@126.com; Ronghua Zhou, 18611073228@163.com

† XM, BY, YZ, FG and RZ contributed equally as co-first authors.

CITATION

Ma X, Yang B, Zheng Y, et al.
Biomechanics of helmet mask structures in mitigating explosion-induced traumatic brain injury: A numerical simulation study.
Molecular & Cellular Biomechanics. 2025; 22(4): 1398.
<https://doi.org/10.62617/mcb1398>

ARTICLE INFO

Received: 19 January 2025

Accepted: 18 February 2025

Available online: 28 February 2025

COPYRIGHT



Copyright © 2025 by author(s).
Molecular & Cellular Biomechanics is published by Sin-Chn Scientific Press Pte. Ltd. This work is licensed under the Creative Commons Attribution (CC BY) license.
<https://creativecommons.org/licenses/by/4.0/>

Abstract: Traumatic brain injury (TBI) caused by explosions is the most common injury suffered by front-line soldiers. However, research on protective gear has primarily been limited to different types of helmets or their internal padding systems. Aerogels, with their microporous structures and high acoustic impedance properties, can effectively buffer the impact of explosions and generate significant acoustic mismatches between adjacent layers, making them promising materials for reducing the damage of blast shock waves to the head. This study aims to enhance the performance of protective equipment in mitigating explosion-induced head injuries and proposes a novel helmet mask structure based on polycarbonate and aerogel laminated composites. The coupled Eulerian-Lagrangian (CEL) method in Abaqus is employed to analyze the mechanical responses of different helmet-mask protective structures under blast shock waves through numerical simulation. The study emphasizes the influence of the type and thickness of the protective structure on head injury. Our findings indicate that a helmet with a face shield can significantly slow down the propagation of the blast wave to the face, thereby reducing craniocerebral injury. Further analysis reveals that the combination of polycarbonate and aerogel layers is more effective than a fully polycarbonate face shield in mitigating intracranial pressure (ICP) in the frontal and parietal regions. Additionally, masks with 3-layer configurations (featuring a single 0.6 mm thick aerogel layer) and 5-layer configurations (with double 0.6 mm thick aerogel layers) performed best in preventing moderate and severe traumatic brain injury (TBI). These results provide a scientific basis and a new direction for the design and optimization of future protective helmets.

Keywords: explosive shock wave; helmet mask; aerogel; polycarbonate; protective effectiveness; numerical simulation

1. Introduction

Approximately 130,000 deployed U.S. soldiers have suffered from traumatic brain injury (TBI) due to the conflicts in Iraq and Afghanistan, and 5% of military personnel experience severe post-traumatic stress disorder. The unequal nature of these battles, where many soldiers were frequently exposed to improvised explosive devices (IEDs) while on duty, was later identified as the primary cause of this high incidence [1–3].

Patients with long-term brain injuries from primary blast shock waves often exhibit symptoms such as temporary respiratory arrest and memory loss. Additional symptoms include headaches, insomnia, sensitivity to light and noise, and potential cognitive impairment [4,5].

Enhancing structural confinement can effectively improve the protective

performance of soldiers' face protection equipment, reducing the impact of shock waves and their superimposed effects [6]. Kang et al. [7] tested the forward and lateral shock wave protection performance of helmet-head systems with varying structures and protection levels, comparing the peak shock wave overpressure and the duration of action in critical areas. Valverde-Marcos et al. [8] evaluated a riot helmet with a well-sealed, double-padded structure under different explosive loads. Their results showed that the helmet significantly reduced cerebral centroid acceleration, intracranial pressure, and cerebellar strain. Zhang et al. [9] investigated the weakening effect of a suspension liner on head load due to shock waves using a three-dimensional head finite element model. They concluded that the foam liner could increase the pulse width, delay and reduce the arrival time of the pressure peak, and provide some protective benefits to the head. Yang et al. [10] conducted an experimental study on the protective performance of explosion-proof helmets under shock wave conditions. Their findings indicated that a full helmet offered the best protection, reducing the overpressure peak by at least 80%, and that improved sealing positively impacted shock wave protection. Rodriguez-Millan et al. [11] examined the effectiveness of a synergistic combination of multiple protective components against generated shock waves. They found that mechanisms such as the addition of highly confined protective structures and the movement and deformation of protective equipment were effective in preventing direct injuries and reducing craniocerebral injuries. Researchers at the Massachusetts Institute of Technology (MIT) [12] installed a mask on a helmet to prevent shock waves from directly reaching the face, which reduced intracranial pressure by up to 60%. Courtney et al. [13] reported that several transparent armor materials, including laminated glass and polycarbonate, absorb and reflect pressure, thereby reducing the transmission of shock waves to the face. Grujicic et al. [14] found that the use of enhanced Advanced Combat Helmets (ACH) had a positive impact on the dynamic load and motion response of the head, reducing intracranial pressure and acceleration, as demonstrated through simulation analysis of unprotected, standard ACH protection, and enhanced ACH protection. In addition to head injuries, facial injuries represent a significant concern in blast or high-impact scenarios. The face is particularly vulnerable to blast shock waves, shrapnel, and secondary impacts, which can lead to severe soft tissue damage, fractures, and long-term functional impairments. While the current study primarily focuses on the biomechanical response of the skull to blast-induced trauma, future research will explore the potential role of helmet mask designs in mitigating facial injuries. This includes evaluating the protective efficacy of visor constructions and the use of advanced materials to enhance overall safety and comfort for the wearer.

In summary, recent research on head protection has primarily focused on various helmet designs or their interior padding systems. However, there has been limited investigation into the use of aerogels and their composites in the structural design of helmet masks.

This study aims to investigate the effectiveness of a polycarbonate-aerogel laminate composite helmet mask in reducing impact-related head injuries. To evaluate the impact of different helmet-mask types and thicknesses on protective performance, the mechanical response of the head under impact is analyzed based on the validation of the helmet-head coupling model. Intracranial pressure (ICP), cranial stress, air

pressure near the face, and mask deformation are used as key evaluation metrics.

2. Methods

2.1. Finite element models

2.1.1. Head-helmet model

As shown in **Figure 1a**, the head model includes the face, cortical bone, trabecula, cerebellar falx, cerebrospinal fluid, scalp, brain, and tentorium. Due to the highly folded nature of the meninges, scalp, and face, a tetrahedral grid is used, while a hexahedral grid is employed for the remaining structures. The head and neck finite element model was validated using Nahum's intracranial pressure experiments [15], Trosseille's intracranial kinetic response experiments [16], and Hardy's relative craniocerebral displacement experiments [17]. These validations demonstrated the model's strong stability and biofidelity, confirming its suitability for assessing head injuries during explosions [18].

In explosion simulations, the face can significantly affect the entry of shock waves into the cranial cavity. Therefore, this simplified model modifies the facial anatomical features to better fit the simulation requirements. The validity of the coupled head-helmet model is verified using the Coupled Eulerian-Lagrangian (CEL) method in Abaqus.

Internal padding systems have been shown to effectively cushion the head and reduce the transmission of shock waves into the head region during an explosion, with different padding systems producing varying results [19,20]. The helmet used in this study is the Kevlar Personnel Armor Systems Ground Forces Helmet, which features an internal padded structure consisting of a shell, padding, helmet straps, harness, and bars. The helmet is equipped with a Hybrid III head model, which was validated in a previous study [21]. A hexahedral mesh is used for the helmet and backrest, while a tetrahedral mesh is employed for the backstrap and crossbar.

The meshing process was conducted using HyperMesh, where Delaunay triangular meshes were initially generated, followed by the creation of tetrahedral meshes to ensure a closed area. To address potential issues with aspect ratio and mesh quality, the Laplace algorithm was applied for mesh refinement. Additional optimization techniques, such as local mesh reconstruction, node insertion, and deletion, were employed to enhance the overall mesh quality. While the current study primarily focuses on the biomechanical response of the skull to blast-induced trauma, future research will explore the potential role of helmet mask designs in mitigating facial injuries. This includes evaluating the protective efficacy of visor constructions and the use of advanced materials to enhance overall safety and comfort for the wearer. Convergence studies were performed to ensure that the mesh was sufficiently fine to capture the peak values reported in the results. The mesh size was progressively refined until the changes in key output parameters (e.g., pressure and stress) were within an acceptable tolerance (less than 2%). This ensured that the simulation results were independent of the mesh size and accurately represented the physical phenomena under investigation. The finite element model of the head and neck components is shown in **Figure 1b**.

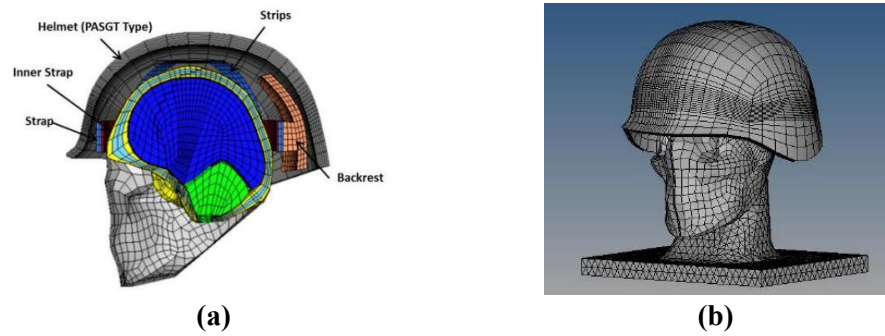


Figure 1. Head and neck model: **(a)** head model anatomy and helmet model interior liner system; **(b)** neck device with tetrahedral mesh.

2.1.2. Mask model

The structure of the mask is illustrated in **Figure 2a** and comprises two primary components: (1) a bracket positioned in the front area of the helmet, and (2) a protective mask with a thickness of 3 mm, which is attached to the bracket. The main objectives of the mask are to absorb impact energy, mitigate the effects of shock waves on the head, and distribute the majority of the impact force away from the face. To ensure complete coverage of the facial region and a seamless integration with the front profile of the helmet, these components were precisely modeled in SolidWorks software and subsequently transferred to the Hypermesh platform for meshing. Given the exceptionally high density of the mask material, the mesh of the mask was divided into at least three layers to avoid convergence issues throughout the study. The full helmet model with the mask is shown in **Figure 2b**, and the mask weighs a total of 511 grams.

The performance of the connecting points between the helmet and mask is another critical aspect of the protective equipment's overall effectiveness. In our simulations, we used the Coupling Constraint feature in Abaqus to model the mechanical connection between the helmet and mask. This approach couples the degrees of freedom of the connection points to a reference point, accurately simulating the actual mechanical interaction. Our results show that the connecting points remain stable under blast loading, with no significant stress concentrations or deformations observed. This ensures that the mask remains securely attached to the helmet, maintaining its protective function even under extreme conditions.

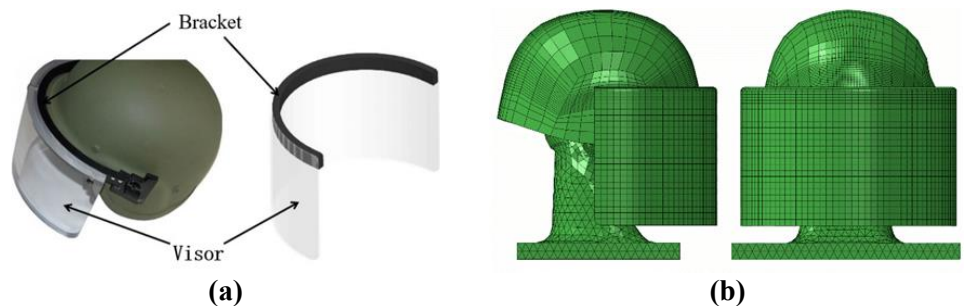


Figure 2. Mask and helmet model: **(a)** mask construction; **(b)** model of a complete helmet with mask.

2.1.3. Material properties

Table 1 presents the material properties for each tissue structure. The mask is made of a polycarbonate-aerogel laminated composite, with the aerogel layer sandwiched between the polycarbonate layers. The neck material is defined as soft tissue, and the facial support is manufactured from aluminum. All component materials are characterized using linear elasticity and isotropy, with the exception of the helmet material, which is defined as anisotropic [22,23].

The protective performance of the mask is evaluated within the limits of its structural strength. The simulation results demonstrate that the mask's design and material properties are sufficient to withstand the blast-induced stresses without failure. This highlights the robustness of the mask's structural design and its ability to provide reliable protection under high-impact conditions.

Table 1. Component material properties.

Component	Density (g/cm ³)	Young's modulus E/(GPa)	Poisson's	Bulk modulus
Rear liner (polyurethane)	0.16	0.057	0.24	-
Helmet	1.23	20/20/7	0.33/0.33/0.77	0.77/2.715/2.715
Leather inner belt	1.153	0.5	0.3	-
Nylon Polyester Tape	1.16	2.4	0.35	-
Bracket (aluminium)	2.70	70	0.35	-
Mask (polycarbonate layer)	1.22	2.4	0.37	-
Mask (aerogel layer)	0.10	0.01	0.2	-

2.2. Air environment

The shock-loaded environment was constructed using a cubic geometry with side lengths of 330 mm. The region was discretized into a hexahedral mesh with a cell size of 3 mm, resulting in a total of 1,331,000 cells.

The domain is filled with air, which is modeled using the properties of an ideal gas. The ideal gas model is chosen because it provides a reasonable approximation of real gas behavior under appropriate conditions, such as low pressure and high temperature, which are typical of blast scenarios in combat fields. The Equation of State for the ideal gas model is expressed as:

$$p = p_A = \rho R(\theta - \theta^Z) \quad (1)$$

where ρ_A is the ambient pressure, R is the gas constant, ρ is the density, θ is the current temperature, and θ^Z is the absolute zero on the temperature scale used.

For the ideal gas model in Abaqus/Explicit, the gas constant R and the ambient pressure ρ_A must be defined. The constant volume specific heat capacity C_V must also be defined, as well as the constant pressure specific heat capacity C_P , as shown in Equation (2).

$$R = C_P - C_V \quad (2)$$

The characteristics used in the simulated air are presented in **Table 2**. In the coupling analysis, air substances are allowed to flow through the air domain, but the elements within this domain are not permitted to deform.

To ensure the relevance of our model to real-world combat scenarios, we have compared the simulated air wave behavior with experimental data from blast events in similar environments. The results demonstrate that the ideal gas model accurately captures the key characteristics of air waves, including pressure propagation and shock front dynamics, under the conditions studied. This validation supports the use of our model for analyzing blast-induced injuries in combat fields.

Table 2. Environment characteristics.

Material	Hourglass control	Density (kg/mm ³)	Dynamic adhesion (Pa·s)	Constant-pressure specific heat (J/(kg·°C))	Environmental pressure (MPa)	Initial ambient temperature (°C)	Gas constant (J/kg·K)
air	tackiness	1.18×10 ⁻⁹	1.8×10 ⁻⁵	1005	0.1	30	287.04

2.3. Boundary conditions

Assuming that the face of the test item serves as the starting point for the explosion shown in **Figure 3**, a non-reflective boundary condition is applied to all surfaces (indicated in blue) in this study, except for the front side of the cubic region containing the helmet model. This boundary condition helps simulate the air pressure distribution generated by the shock wave by creating suction during the negative pressure phase, which draws air back toward the explosion source.

Since the head and helmet models are lighter than the rest of the body, the pressure from the impact loads during the analysis could cause displacements and accelerations that differ from real-world conditions. To prevent such unrealistic shoulder rotations and displacements, boundary conditions are applied at the neck.

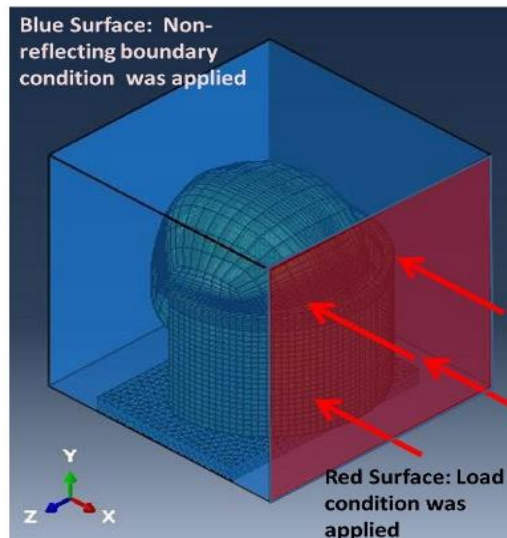


Figure 3. Non-reflective boundary and loading conditions.

2.4. Load conditions

This study assumes that the shock waveform characteristics generated by TNT can be approximated by the Friedlander waveform equation [24].

$$P = P_s e^{-\left(\frac{t}{t^*}\right)} \left(1 - \frac{t}{t^*}\right) \quad (3)$$

where P_s is the peak pressure, t^* is the time when the pressure first crosses the

horizontal axis (before the negative phase).

A peak overpressure of 1 atmosphere was applied, occurring at 0.05 ms. According to the aforementioned equation, the positive pressure gradually decreases and transitions to a negative phase at approximately 0.15 ms, with the pulse ending around 0.85 ms. This loading condition acts on the entire front surface of the cubic region, enabling the simulation of a planar explosion.

2.5. Simulation cases

For this study, a total of five scenarios with a run time of two milliseconds are established. The material and form of the mask are varied in all but one of the head models, which is without a mask. The specific cases are as follows:

- Case 1: A helmet without a mask.
- Case 2: A helmet with a fully polycarbonate mask.
- Case 3: A helmet with a composite mask featuring a three-layer structure, including a 0.6 mm aerogel layer.
- Case 4: A helmet with a composite mask featuring a three-layer structure, including a 1.2 mm aerogel layer.
- Case 5: A helmet with a composite mask featuring a five-layer structure, consisting of two composite masks, each with a 0.6 mm aerogel layer, maintaining a total thickness of 3 mm.

3. Results and discussion

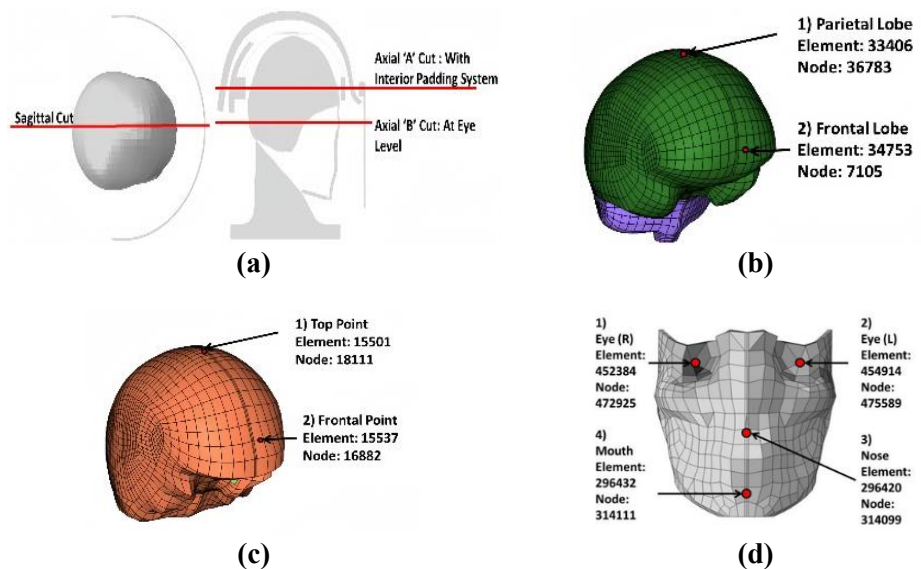


Figure 4. Measuring the node position: (a) planar cuts for coronal view explosion sequences; (b) ICP Assessment node; (c) skull stress assessment node; (d) near-surface air pressure evaluation node.

In this research, three distinct cutting planes are utilized based on the finite element models, boundary conditions, and scenarios described above. As shown in **Figure 4a**, the planar “A” cut provides an axial view from the top to examine the interaction between the shock wave, the helmet, its internal cushioning system, and

the head. The sagittal incision is used to evaluate the side view of the contour. The “B” cutting plane allows for a deeper understanding of how the shock wave interacts with the mask and the face.

During the investigation, two distinct locations in the brain’s frontal and parietal lobes were randomly selected to assess the impact of the explosion on intracranial pressure. Regarding the skull, as illustrated in **Figure 4b,c**, the von Mises stresses at the anterior and vertex positions are measured to examine the impact of the shock wave on the skull. Finally, as shown in **Figure 4d**, air pressure readings are collected at four distinct locations near the face to investigate the effects of air pressure on the mouth, nose, and eyes.

3.1. Maskless model response analysis

The parametric analysis of the helmet model with a mask is the focus of this study. To ensure the accuracy of the results, it is essential to compare the simulation outcomes of the helmet model without a mask to those of the simulations that include an air pressure peak overpressure impact load.

3.1.1. Shock wave propagation process

The air pressure around the helmet model changes as shock waves propagate, as seen in **Figure 5a**. Air pressure above 0.5 MPa is indicated in red, while air pressure near ambient levels or negative pressure is shown in blue. According to the analysis, a shock wave reaches the face at 0.20 ms. At the same time, the shock wave in front of the helmet begins to reflect, and the extent of this reflection becomes clearly visible after 0.10 ms, indicating that the shock wave does not directly impact the skull.

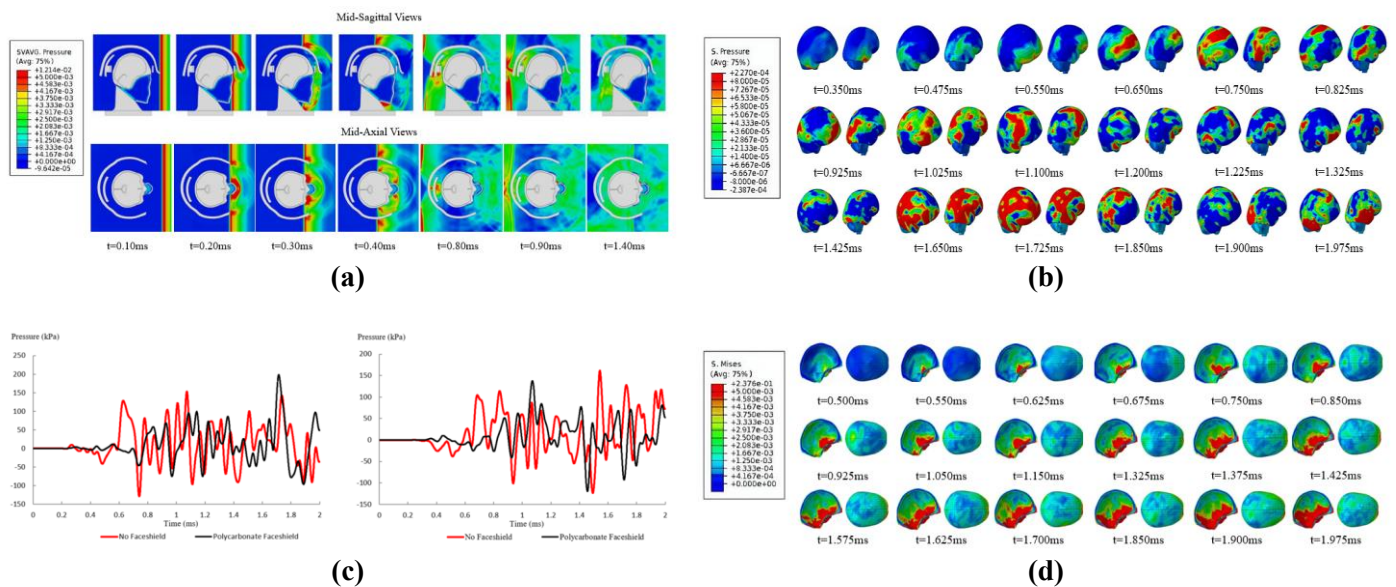


Figure 5. Intracranial pressure, cranial stress map without mask: **(a)** shock wave propagation without mask; **(b)** ICP profile of the without mask model; **(c)** comparison of frontal and parietal lobes with and without mask intracranial pressure; **(d)** stress diagram of skull without mask.

As shown in **Figure 5a**, the shock wave also concentrates under the chin, where it bypasses the head and causes a secondary impact on the hindbrain and occipital lobe between 0.70 ms and 0.85 ms. The shock wave enters the helmet through the earmuff

portion, leading to a high concentration of air pressure in the temporal region. At 1.05 ms, the shock wave starts to return to the front due to the negative pressure generated by the shock loading, which causes the surrounding air to be drawn forward.

3.1.2. Intracranial pressure and cranial stress

As illustrated in **Figure 5b**, high pressure first emerges in the temporal lobe around 0.350 ms and does not develop in the frontal lobe until approximately 0.550 ms. Between 0.550 ms and 0.925 ms, there is a significant transfer of intracranial pressure (ICP) from the frontal brain to the occipital cortex.

The intracranial pressure (ICP) curves for the model without a mask are depicted in **Figure 5c**. The frontal lobe experiences an initial ICP value of 122 kPa at approximately 0.6 ms. During the simulation, the frontal lobe then undergoes several peaks of positive and negative pressure exceeding 100 kPa, and the parietal lobe exhibits a similar pattern. The ICP plot indicates that the shock wave travels from the front to the back of the brain, and **Figure 5c** also illustrates the time delay of the initial positive pressure peak, showing that the shock wave moves from the frontal to the parietal lobes in about 0.08 ms.

Figure 5d shows that stress propagates from the anterior to the posterior part of the skull between 0.500 ms and 1.050 ms, and then returns to the anterior at 1.150 ms due to air inhalation. High-stress regions are located on the lateral side of the skull, starting at the bottom front and extending to the bottom rear.

3.1.3. Validation of results

To validate the results, the maximum values of cranial stress and the peak ranges of intracranial pressure (ICP) were compared with those from previous investigations. The ICP ranges for the frontal and parietal lobes are -0.119 MPa to 0.154 MPa and -0.119 MPa to 10.161 MPa, respectively.

Previous research has shown that minor variations in the head model's geometry, the helmet's interior padding arrangement, and the material's composition can influence the values of cranial stress and ICP. Grujicic et al. [25] conducted a study in a 0.1 MPa (1 atm) peak overpressure TNT explosion environment and found that their helmet model recorded ICP values between -0.08 MPa and 0.08 MPa. In another study, Zhang et al. [26] reported that the peak ICP for a 0.27 MPa (2.7 atm) peak overpressure TNT explosion environment in a helmeted condition was 0.6 MPa. The study by Tan et al. [27] were based on a 0.1 MPa peak overpressure, and their simulations showed cranial stress values of 6 MPa and 11 MPa for two different helmet configurations. In the present study, the stress at the front and top of the skull was measured to be 4.37 MPa and 2.71 MPa, respectively.

3.2. Model response analysis with mask

3.2.1. Shock wave propagation process

As seen in **Figure 6a**, the shock wave begins to strike the mask at 0.10 ms. Between 0.20 ms and 0.30 ms, the mask prevents the shock wave from directly impacting the face. However, due to its small thickness and short length, the mask is unable to completely stop the diffracted shock wave from entering the face.

The mask diffracts the majority of the shock wave and significantly delays the time it takes for the shock wave to reach the helmet earmuffs, from 0.10 ms to 0.65

ms, compared to the situation without the mask. The area of high pressure between the head and the helmet is considerably reduced with the mask, and there is a lesser secondary effect at the occipital lobe when comparing the air pressure profiles in these two scenarios.

However, over time, the negative pressure generated by the impact loading effect causes air to be drawn in, accumulating high pressure between the mask and the face. This high pressure reflects multiple times, potentially lasting for more than 2 ms.

3.2.2. Intracranial pressure and cranial stresses

As shown in **Figure 6b**, the initial intracranial pressure (ICP) values in the temporal lobe decrease from 0.350 ms to 0.475 ms in the presence of the mask. Additionally, the intracranial pressure in the frontal lobe is notably lower in the scenario without the mask compared to the 0.650 ms frame. However, when a mask is worn, elevated ICP is observed in both the frontal and temporal lobes between 1.900 ms and 1.975 ms. This increase in ICP could be attributed to the collection and back-and-forth reflection of stagnant air between the face and the mask.

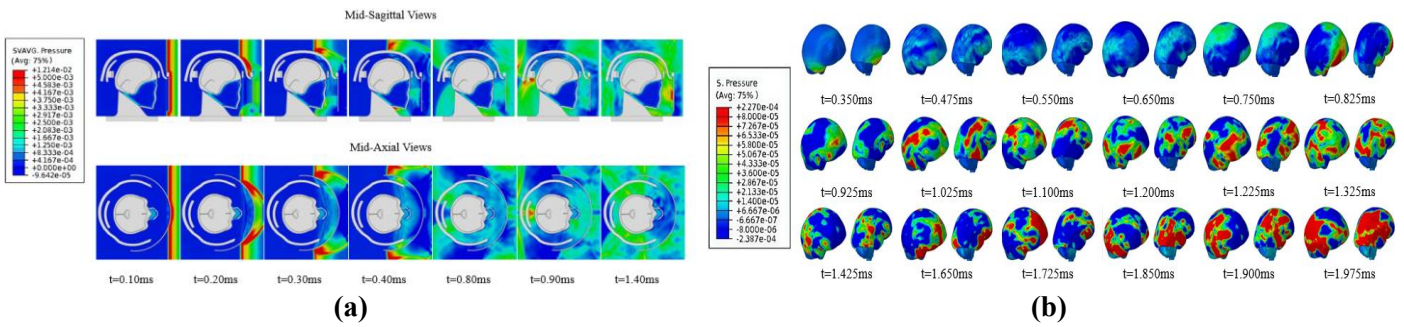


Figure 6. Shock wave propagation with mask: **(a)** shock wave propagation with mask; **(b)** ICP profiles with mask.

As shown in **Table 3**, although the mask is capable of diffracting the shock wave and significantly reducing the intracranial pressure (ICP) at 0.61 milliseconds (the initial overpressure peak in the condition without a mask), the ICP while wearing a mask is still higher and appears after 1.71 ms. This is because, at approximately 1.50 ms, the reflected shock wave and diffraction wave, as seen in **Figure 6b**, begin to generate structural disturbances near the helmet’s ear region. These amplified shock waves then propagate forward, causing severe damage to the frontal lobe. Adjusting the mask’s size, such as extending the side ends, can prevent these structural disturbances from occurring.

Table 3. Frontal intracranial pressure.

Frontal intracranial pressure	Maximum pressure (10^{-3} MPa)	Period of time (ms)
Without mask	154	1.54
Polycarbonate mask	194	1.71

As indicated in **Table 4**, the amplification effect of the shock wave appears not to reach the parietal lobe. In the scenario with the mask, the maximum and minimum ICP values of the parietal lobe are lower, suggesting that the stress caused by the structural disturbance is concentrated behind the parietal lobe.

Table 4. Parietal intracranial pressure.

Parietal intracranial pressure	Maximum pressure (10^{-3} MPa)	Period of time (ms)
Without mask	161	1.54
Polycarbonate mask	134	1.07

The first peak stress in the mask model was lower for both skull positions compared to the without mask case, indicating that the mask’s ability to diffract waves helps to reduce the impact of shock waves on the skull. Nonetheless, it is evident that the face mask causes more stress at the front of the skull, and the maximum stress in both locations occurs after 1.91 ms. As seen in **Figure 7a**, this may be due to the buildup of air pressure between the mask and the face.

From the stress wave propagation depicted in **Figure 7a,b**, the propagation direction and intensity are similar in both scenarios. However, when a mask is worn, the pressure on the side of the skull is reduced. The analysis results from **Figure 7b** are summarized in **Tables 5** and **6**.

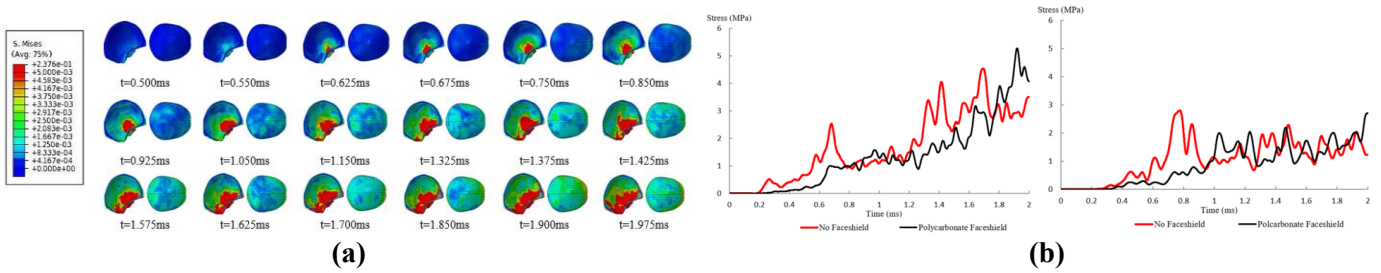


Figure 7. Intracranial pressure, cranial stress map without mask: **(a)** cranial stress maps with mask; **(b)** comparison of skull stress between anterior points and apex with or without mask.

Table 5. Cranial anterior point stresses.

Cranial anterior point stress	Maximum pressure (MPa)	Period of time (ms)
Without mask	4.37	1.68
Polycarbonate mask	5.18	1.91

Table 6. Stresses on the top of the skull.

Cranial vertex stress	Maximum pressure (MPa)	Period of time (ms)
Without mask	2.71	1.54
Polycarbonate mask	2.59	2.00

3.2.3. Facial air pressure

As shown in **Figure 8**, between 0.2 ms and 0.4 ms, the mask diffracts the shock wave when it hits the model, significantly reducing the air pressure near three key points on the face.

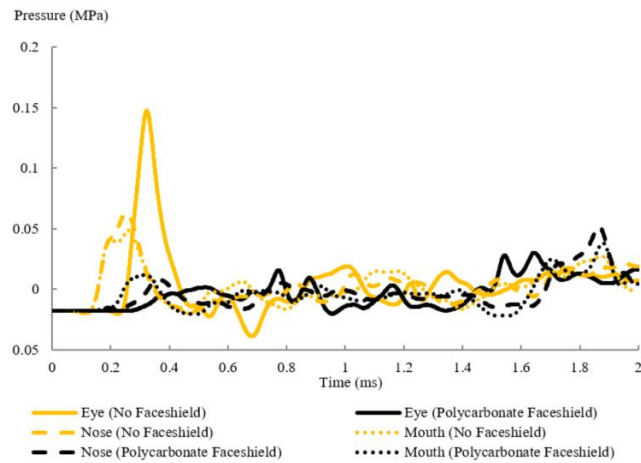


Figure 8. Comparison of air pressure underneath the mask with and without the mask.

3.3. Response analysis of different protective masks

3.3.1. Intracranial pressure and cranial stresses

As can be observed from the graphs in **Figure 9a,b**, the intracranial pressure (ICP) in the frontal and parietal lobes of all structures remains the same until 0.9 ms. After the impact load front has passed through the head, the pressure is drawn back by the resulting negative pressure.

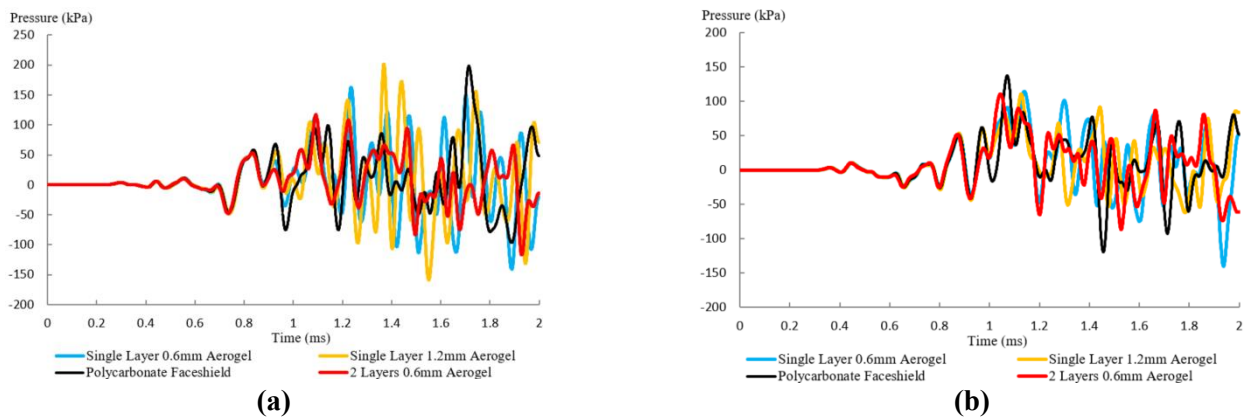


Figure 9. Frontal and parietal intracranial pressures for different mask configurations: **(a)** frontal intracranial pressure; **(b)** Parietal intracranial pressure.

As illustrated in **Table 7**, all-polycarbonate laryngeal masks (without aerogel) exhibit a delayed gas buildup but ultimately lead to an increase in prefrontal intracranial pressure (ICP). Notably, a single-layer 0.6 mm aerogel laryngeal mask demonstrates superior performance compared to a single-layer 1.2 mm aerogel mask. However, when the 1.2 mm aerogel is divided into two 0.6 mm layers and integrated into a five-layer structure, it achieves a 28% reduction in prefrontal ICP. This multi-layered configuration proves to be the most effective in mitigating the impact of shock waves. The severity of Traumatic Brain Injury (TBI) is commonly evaluated based on ICP tolerance thresholds. According to established medical standards, severe TBI is typically diagnosed when the maximum ICP exceeds 235 kPa, while mild or no TBI is indicated when the ICP remains below 173 kPa [28]. Our simulation results reveal

that exposure to a 0.1 MPa shock wave can induce severe TBI in the absence of protective mask coverage. However, the application of full polycarbonate masks or single-layer 1.2 mm aerogel masks reduces the severity to moderate TBI. More advanced protective measures, such as multi-layered masks (e.g., three or five layers) or masks redesigned to disperse shock waves and prevent barometric pressure buildup, provide significantly enhanced protection. These innovative designs effectively mitigate brain damage caused by shock loading, highlighting their potential as highly effective countermeasures against TBI.

Table 7. Frontal ICP for different mask configurations.

Type	Maximum pressure (10^{-3} Pa)	Period of time (ms)	Minimum pressure (10^{-3} MPa)	Period of time (ms)
Polycarbonate masks	194	1.71	-85	1.87
Single layer 0.6 mm aerogel	159	1.23	-132	1.88
Single layer 1.2 mm aerogel	201	1.37	-154	1.55
Double layer 0.6 mm aerogel	110	1.09	-135	1.88

As demonstrated in **Table 8**, both single-layer 1.2 mm aerogel masks and double-layer 0.6 mm aerogel masks exhibited identical maximum pressures, with the lowest pressures observed in the parietal lobe. Notably, when comparing a single-layer 1.2 mm aerogel mask with a double-layer 0.6 mm aerogel mask under masked conditions, the parietal intracranial pressure (ICP) was reduced by up to 35%. For three-layer masks, the thicker aerogel layer demonstrated superior performance in the parietal lobe compared to the frontal lobe. However, the most effective reduction in ICP across both frontal and parietal regions was achieved by combining an aerogel mask with an all-polycarbonate mask. This hybrid configuration significantly mitigated the impact load-induced ICP, highlighting its potential as an optimal protective design.

Table 8. Parietal ICP for different mask configurations.

Type	Maximum pressure (10^{-3} MPa)	Period of time (ms)	Minimum pressure (10^{-3} MPa)	Period of time (ms)
Polycarbonate masks	133	1.07	-116	1.44
Single layer 0.6 mm aerogel	114	1.14	-133	1.93
Single layer 1.2 mm aerogel	104	1.12	-56	1.79
Double layer 0.6 mm aerogel	104	1.04	-80	1.51

As shown in **Figure 10a,b**, and **Table 9**, a thinner aerogel layer (0.6 mm) more effectively mitigates the impact effect at the anterior point, while a thicker aerogel layer (1.2 mm) better reduces the impact effect at the apex. The double-layer 0.6 mm aerogel mask is more effective in reducing the stress at the anterior point of the skull, whereas the single-layer 1.2 mm aerogel mask significantly reduces the stress at the apex of the skull. Regarding cranial stress, McElhaney et al. [29] conducted a systematic analysis of the mechanical properties of the cranium, including its modulus of elasticity, compressive strength, flexural strength, and fracture toughness, with a particular focus on the stress-strain behavior under various loading conditions. Their study established a range of stress thresholds for cranial fractures, spanning from 34.47 to 103.42 MPa. In our simulations, the blast shock wave did not induce skull fractures

when a helmet mask was worn, as the resulting stress levels remained below the fracture thresholds identified by McElhaney et al. This finding underscores the protective efficacy of helmet masks in mitigating cranial injuries under blast conditions, demonstrating their critical role in safeguarding against trauma.

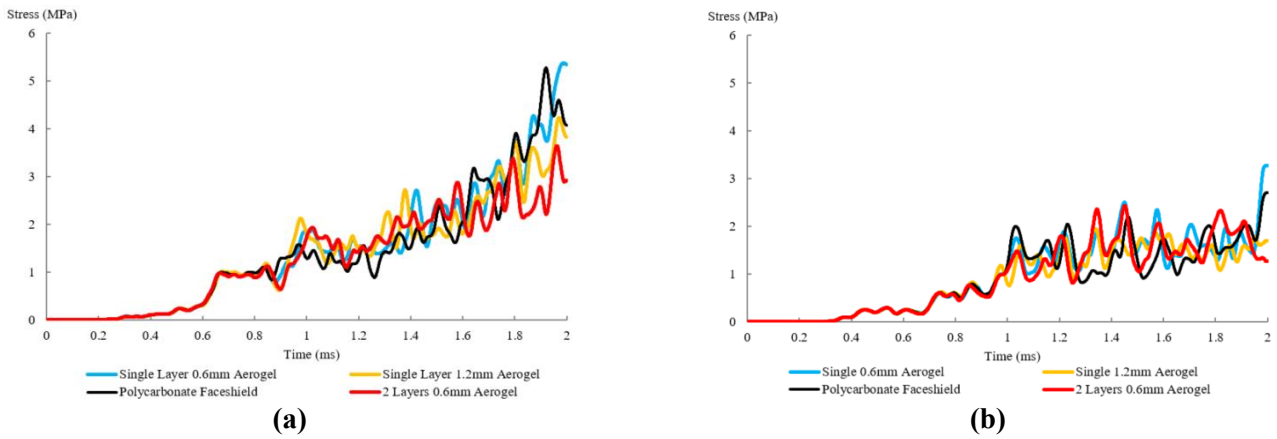


Figure 10. Anterior and vertex cranial stresses in different mask configurations: **(a)** skull stress at the anterior point; **(b)** skull stress at the anterior point.

Table 9. Cranial stresses for different mask configurations.

	Maximum stress at the front point (MPa)	Period of time (ms)	Maximum Vertex Stress (MPa)	Period of time (ms)
Polycarbonate masks	5.18	1.91	2.59	2
Single layer 0.6 mm aerogel	5.28	1.97	3.19	1.98
Single layer 1.2 mm aerogel	4.34	1.95	1.36	1.83
Double layer 0.6 mm aerogel	3.63	1.95	2.299	1.44

3.3.2. Facial air pressure

As shown in **Figure 11a,b**, with the exception of the completely polycarbonate mask, all other control groups had approximately the same air pressure at the mouth and nose. However, **Figure 11c** illustrates that the mask structure had a more significant impact on the air pressure at the eyes. **Table 10** indicates that the single-layer 1.2 mm aerogel mask recorded the lowest maximum air pressure and effectively diffracted the shock wave, with air accumulation between the mask and the face occurring at around 1.65 ms. Additionally, the double-layer 0.6 mm aerogel mask exhibited maximum and minimum pressures at intervals of 0.85 ms and 1.10 ms, respectively. In contrast, the pressure maxima and minima for the other masks were not observed until the air pressure inside the mask began to increase. This difference suggests that the five-layer structure may result in lower intracranial pressure (ICP) and cranial stresses because it is more effective at diffracting the stronger frontal shock wave.

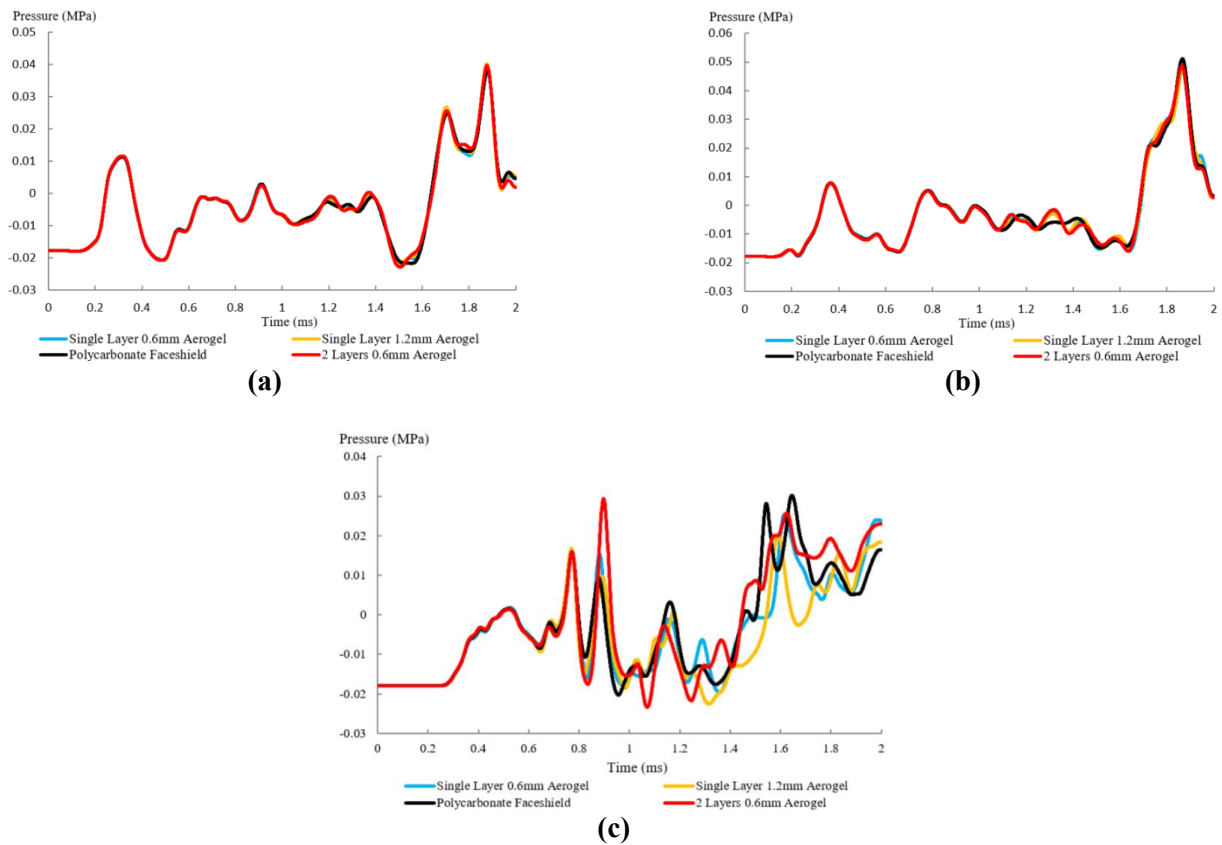


Figure 11. Air pressure at different parts of the attachment for different mask configurations: **(a)** air pressure in the vicinity of the mouthpiece; **(b)** air pressure near the nose; **(c)** air pressure near the eyes.

Table 10. Air pressure near the eye for mask configuration.

Air pressure near the eyes	Maximum pressure (MPa)	Period of time (ms)	Minimum pressure (MPa)	Period of time (ms)
Polycarbonate masks	0.029	1.64	-0.019	0.94
Single layer 0.6 mm aerogel	0.023	1.97	-0.020	1.34
Single layer 1.2 mm aerogel	0.019	1.58	-0.022	1.29
Double layer 0.6 mm aerogel	0.028	0.89	-0.025	1.06

3.3.3. Mask deflection

The mask’s deflection is a crucial measure of its overall stiffness and shock-absorbing capacity. Furthermore, the degree of deflection influences how the shock wave spreads from critical areas of the skull. Therefore, it is essential to study the role of mask deflection in reducing shock loads.

In addition to deflection, the stress levels and structural strength of the mask are critical factors in evaluating its protective performance. The mask material, polycarbonate, has a yield strength of approximately 62 MPa and an ultimate tensile strength of 72 MPa. Our simulation results indicate that the maximum von Mises stress experienced by the mask under blast loading conditions remains well below these thresholds, ensuring that the mask does not undergo plastic deformation or failure. This analysis confirms that the mask’s structural design is capable of withstanding the blast-induced stresses, providing effective protection while maintaining its integrity.

Figure 12 shows the deflection amounts for three different mask configurations.

At 0.30 ms and 0.70 ms, deflection is observed at the center of the mask, followed by significant deformation at the bottom. At 1.00 ms, high deflection occurs at the position where the mask aligns with the eye. From 1.40 ms onwards, inward deflection occurs across the mask region, with the highest deflection again occurring at the bottom. According to the deflection contours in **Figure 13a**, two high deflection points are identified, and **Figure 13b** indicates that the maximum deflection of the mask occurs at the second point at the bottom of the mask. Based on the cantilever bending hypothesis, this suggests that the highest deflection occurs farthest from the fixed point.

Using point 2 as an example, the mask's deflection was measured, and the results are displayed in **Figure 13c**. The figure shows that the deflection pattern is consistent across all configurations, with the maximum deflection occurring around 0.6 ms. The deflection decreases between 0.60 ms and 0.95 ms, which aligns with the shock wave propagation depicted in **Figure 6a**, where the shock wave is diffracted by the mask, reducing the pressure exerted on it. The mask then deflects inward again between 1.00 ms and 1.30 ms, coinciding with the presence of negative pressure at the impact load's center, which pulls air in front of the mask. Simultaneously, the air flowing through the model is drawn towards the mask by the negative pressure, leading to a decrease in deflection.

By comparing the deflection graphs of different mask structures, we can conclude that the single-layer 0.6 mm aerogel mask has the lowest peak deflection, indicating that it is the stiffest. This stiffness may also explain the relatively high intracranial pressure (ICP) and cranial stresses associated with this construction, as the rigid mask allows air pressure to build up between the face and the mask before entering the cranial cavity.

Moreover, the deflection behavior of the five-layer structural mask appears erratic between 1.2 ms and 2.0 ms, with the lowest deflection occurring between 1.2 ms and 1.6 ms and the highest deflection occurring between 1.6 ms and 2.0 ms. The variation in deflection during these two time periods is more pronounced than in the three-layer structure. The different degrees of deflection cause the shock wave to diffract differently, which enhances shock mitigation in the frontal, parietal, and anterior regions of the skull.

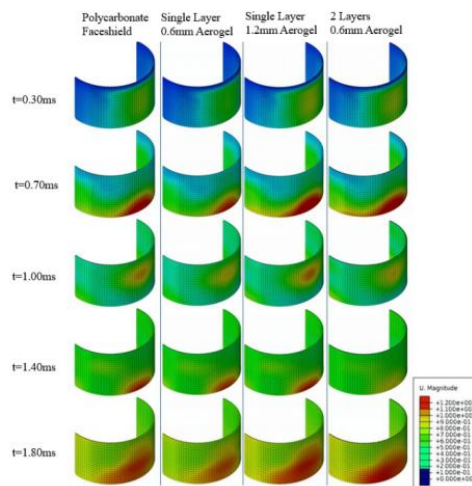


Figure 12. Inward deflection profile on shield for different shield configurations.

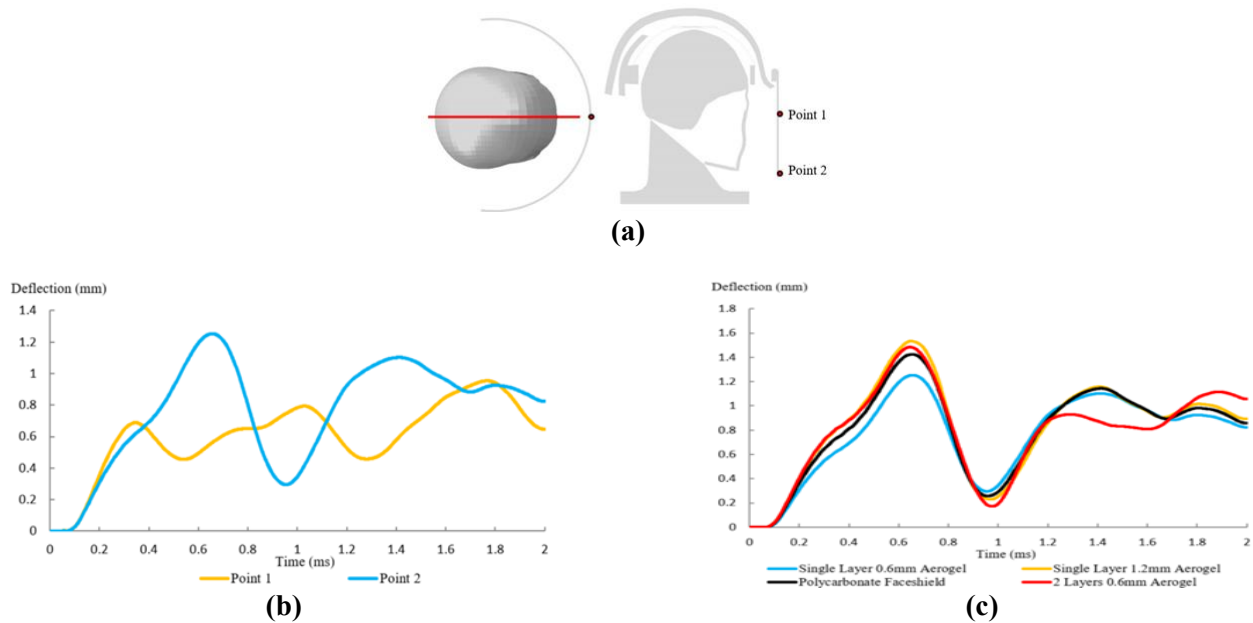


Figure 13. Pressure at different deflection points on the mask: **(a)** deflection point on the mask; **(b)** single 0.6 mm aerogel mask deflected inwards at points 1 and 2; **(c)** inward deflection of different mask structures at point 2.

3.4. Limitations

While the current study focuses on frontal blast impacts, it is important to acknowledge that real-world blast events often involve oblique or slanted shock waves, including those originating from the ground. These conditions can significantly alter the injury mechanisms and peak values due to the breaking of symmetry and the reflection of shock waves.

In this study, the boundary conditions applied to the neck restrict displacement and rotation of the ‘shoulders,’ limiting the analysis to frontal impacts. However, we recognize the critical need to investigate the effects of oblique impacts and ground-reflected shock waves on cranial injuries and helmet performance.

Future work will expand the scope of the analysis to include slanted shock waves in both the vertical and horizontal planes. This will involve modeling the interaction of blast waves with the ground and their reflection, as well as evaluating the protective efficacy of helmet designs under these more complex conditions. Such studies will provide a more comprehensive understanding of blast-induced traumatic brain injury and inform the development of improved protective equipment.

4. Conclusion

Through numerical simulation, the protective effect of polycarbonate and aerogel material helmet mask structures under shock waves was investigated. The validity of the head-helmet coupling model was confirmed by comparing it with experimental data from the literature, leading to the following conclusions:

1) Response evaluations comparing helmet models with and without a 3 mm polycarbonate mask revealed that the ICP in the frontal lobe could be effectively reduced with a helmet that included a mask from the beginning of the explosion until 1.5 ms. However, after this point, the negative pressure of the blast wave drew gases

in and accumulated them between the face and the mask, raising ICP values compared to the scenario without a mask. This similar behavior was observed in studies on the impact of blast waves on the cranium. When examining the effects of bomb impact on the skull, the same phenomenon was noted. However, the mask significantly reduced the pressure near the face and the parietal lobe.

2) Using a 0.6 mm thick single layer of aerogel, a 1.2 mm thick single layer of aerogel, and a double layer of 0.6 mm thick aerogel sandwiched between polycarbonate layers, the total thickness of the mask reached 3 mm. Numerical simulation results showed that increasing the thickness of the aerogel in the three-layer mask structure better relieved the air pressure in the parietal lobe, two skull observation points, and near the eyes. Additionally, due to the potential deflection and shock wave diffraction of the mask, the five-layer mask configuration—comprising two 0.6 mm layers of aerogel—was most effective in reducing the effects of shock loading on the frontal, parietal, and anterior regions of the skull. For lowering the ICP in the frontal and parietal lobes, the combination of polycarbonate and aerogel layers performed better than a solid polycarbonate mask.

3) This study employs numerical simulation to elucidate the mechanical response mechanism of the helmet-mask structure subjected to blast shock waves. The findings establish a robust theoretical foundation for the design and enhancement of protective equipment, while offering scientifically grounded guidance for optimizing its practical application. To further validate and refine the results, future work will focus on verifying the numerical simulations with experimental data from controlled explosion tests, thereby enhancing the accuracy and reliability of the model. Additionally, the exploration of novel lightweight and high-strength materials—such as advanced composites or smart materials—will be pursued to improve the helmet mask's impact resistance and wearer comfort, paving the way for next-generation protective equipment designs.

Author contributions: Conceptualization, XM, BY, YZ, FG, RZ, JZ and XZ; methodology, XM, BY, YZ, FG and RZ; software, XM, BY, YZ, FG and RZ; writing—original draft preparation, XM, BY, YZ, FG and RZ; visualization, XM, BY, YZ, FG and RZ; investigation, JZ and XZ; validation, writing—review and editing, JZ and XZ; supervision, JZ and XZ. All authors have read and agreed to the published version of the manuscript.

Funding: National Natural Science Foundation of China (Grant No. 12372079), the Natural Science Foundation of Jiangsu Province, China (Grant No. BK20201470), Nanjing University of Engineering Graduate Student Science and Technology Innovation Fund Project (No. TB202417038).

Acknowledgments: We thank Heowpueh Lee, Kwongming Tse, and Longbin Tan, Laboratory of Applied Mechanics, National University of Singapore, and Vehicle Engineering Laboratory, Nanjing University of Engineering, for their help in this paper.

Ethical approval: Not applicable.

Conflict of interest: The authors declare no conflict of interest.

References

1. Eynde JO, Yu AW, Eckersley CP, et al. Primary blast wave protection in combat helmet design: A historical comparison between present day and World War I. *PLOS ONE*. 2020; 15(2): e0228802. doi: 10.1371/journal.pone.0228802
2. Li Y, Lin J, Liu S, et al. Experimental and numerical study on the protective mechanism of the full helmet subjected to blast loadings. *Thin-Walled Structures*. 2024; 198: 111666. doi: 10.1016/j.tws.2024.111666
3. Yang B, Sun H, Wang A, et al. A Study on the Finite Element Model for Head Injury in Facial Collision Accident. *Molecular & Cellular Biomechanics*. 2020; 17(1): 49-62. doi: 10.32604/mcb.2019.07534
4. Tse KM, Holder D. A Biomechanical Evaluation of a Novel Airbag Bicycle Helmet Concept for Traumatic Brain Injury Mitigation. *Bioengineering*. 2021; 8(11): 173. doi: 10.3390/bioengineering8110173
5. Huang X, Chang L, Zhao H, et al. Study on craniocerebral dynamics response and helmet protective performance under the blast waves. *Materials & Design*. 2022; 224: 111408. doi: 10.1016/j.matdes.2022.111408
6. Liu ZL, Du ZB, Zhang JR, et al. Progress in the mechanism and protection of blast-induced traumatic brain injury. *Explosion and Shock Waves*. 2022; 42(4): 041101. doi: 10.11883/bzycj-2021-0053
7. Kang Y, Zhang SZ, Zhang YP, et al. Research on anti-shock wave performance of the protective equipment for the head of a soldier based on shock tube evaluation. *Explosion and Shock Waves*. 2021; 41(8): 085901. doi: 10.11883/bzycj-2020-0395
8. Valverde-Marcos B, Rubio I, Antona-Makoshi J, et al. Numerical Analysis of EOD Helmet under Blast Load Events Using Human Head Model. *Applied Sciences*. 2020; 10(22): 8227. doi: 10.3390/app10228227
9. Zhang TG, Satapathy SS. Effect of Helmet Pads on the Load Transfer to Head Under Blast Loadings. Volume 3: *Biomedical and Biotechnology Engineering*. 2014. doi: 10.1115/imece2014-37143
10. Yang WU, Bin Q, Shu W, et al. Helmet protection based on explosive shock waves. *Acta Armamentarii*. 2022; 43(9): 8. doi: 10.12382/bgxb.2022.0553
11. Rodríguez-Millán M, Tan LB, Tse KM, et al. Effect of full helmet systems on human head responses under blast loading. *Materials & Design*. 2017; 117: 58-71. doi: 10.1016/j.matdes.2016.12.081
12. Nyein MK, Jason AM, Yu L, et al. In silico investigation of intracranial blast mitigation with relevance to military traumatic brain injury. *Proceedings of the National Academy of Sciences*. 2010; 107(48): 20703-20708. doi: 10.1073/pnas.1014786107
13. Courtney ED, Courtney AC, & Courtney MW. Blast wave transmission through transparent armour materials. *Journal of Battlefield Technology*. 2012.
14. Grujicic M, Ramaswami S, Snipes J, et al. RETRACTED: Potential improvement in helmet blast-protection via the use of a polyurea external coating: Combined experimental/computational analyses. *Proceedings of the Institution of Mechanical Engineers, Part L: Journal of Materials: Design and Applications*. 2016; 234(3): 337-367. doi: 10.1177/1464420716644472
15. Nahum AM, Smith R, Ward CC. Intracranial Pressure Dynamics During Head Impact. *SAE Technical Paper Series*. 1977. doi: 10.4271/770922
16. Trosseille X, Tarrière C, Lavaste F, et al. Development of a F.E.M. of the Human Head According to a Specific Test Protocol. *SAE Technical Paper Series*. 1992. doi: 10.4271/922527
17. Hardy WN, Foster CD, Mason MJ, et al. Investigation of Head Injury Mechanisms Using Neutral Density Technology and High-Speed Biplanar X-ray. *SAE Technical Paper Series*. 2001. doi: 10.4271/2001-22-0016
18. Tse KM, Tan LB, Lee SJ, et al. Development and validation of two subject-specific finite element models of human head against three cadaveric experiments. *International Journal for Numerical Methods in Biomedical Engineering*. 2013; 30(3): 397-415. doi: 10.1002/cnm.2609
19. Li Y, Fan H, Gao XL. Ballistic helmets: Recent advances in materials, protection mechanisms, performance, and head injury mitigation. *Composites Part B: Engineering*. 2022; 238: 109890. doi: 10.1016/j.compositesb.2022.109890
20. Rodriguez-Millan M, Rubio I, Burpo FJ, et al. Impact response of advance combat helmet pad systems. *International Journal of Impact Engineering*. 2023; 181: 104757. doi: 10.1016/j.ijimpeng.2023.104757
21. Tan LB, Tse KM, Lee HP, & Tan VBC. Ballistic impact analysis on the advanced combat helmet (ACH) -testing and simulation. In: *Proceedings of the 9th Composite Science and Technology (ICCST)*; 2013.
22. Ganpule S, Alai A, Plougonven E, et al. Mechanics of blast loading on the head models in the study of traumatic brain injury using experimental and computational approaches. *Biomechanics and Modeling in Mechanobiology*. 2012; 12(3): 511-531. doi: 10.1007/s10237-012-0421-8
23. Huang X, Zheng Q, Chang L, et al. Study on protective performance and gradient optimization of helmet foam liner under

- bullet impact. *Scientific Reports*. 2022; 12(1). doi: 10.1038/s41598-022-20533-9
24. Dewey JM. The shape of the blast wave: studies of the Friedlander equation. In: *Proceedings of the 21st International Symposium on Military Aspects of Blast and Shock*: 1-9; October 3-8, 2010; Jerusalem, Israel.
 25. Grujicic A, LaBerge M, Grujicic M, et al. Potential Improvements in Shock-Mitigation Efficacy of a Polyurea-Augmented Advanced Combat Helmet. *Journal of Materials Engineering and Performance*. 2011; 21(8): 1562-1579. doi: 10.1007/s11665-011-0065-3
 26. Zhang L, Makwana R, Sharma S. Comparison of the head response in blast insult with and without combat helmet. In: *Proceedings of HFM-207 Symposium on a Survey of Blast Injury across the Full Landscape of Military Science NATO OTAN Research & Technology Organization*: 1-18; 2011.
 27. Tan LB, Lee HP, & Tan VBC. Performance evaluation and design improvement of interior cushioning system of ballistic helmets. Singapore: National University of Singapore, Report for the DSO National Laboratories, Defence Medical and Environmental Research Institute (DMERI); 2012.
 28. Ward C, Chan M, Nahum A. Intracranial Pressure—A Brain Injury Criterion. *SAE Technical Paper Series*. 1980. doi: 10.4271/801304
 29. McElhaney JH, Fogle JL, Melvin JW, et al. Mechanical properties of cranial bone. *Journal of biomechanics*. 1970; 3(5): 495-511. doi: 10.1016/0021-9290(70)90059-X